Nat. Hazards Earth Syst. Sci. Discuss., 1, 3935–3965, 2013
www.nat-hazards-earth-syst-sci-discuss.net/1/3935/2013/
doi:10.5194/nhessd-1-3935-2013

Natural Hazards and Earth System Sciences
Open Access
Discussions

Numerical simulation of levee breach by overtopping in a flume with 180° bend

S.-T. Dou[1,2], D.-W. Wang[3], M.-H. Yu[4], and Y.-J. Liang[5]

[1]Cold and Arid Regions Environmental and Engineering Research Institute, Chinese Academy of Sciences, 73000 Lanzhou, China
[2]Yellow River Institute of Hydraulic Research, YRCC, 450003 Zhengzhou, China
[3]State Key Laboratory of Simulation and Regulation of River Basin Water Cycle, China Institute of Water Resources and Hydropower Research, 100038 Beijing, China
[4]State Key Laboratory of Water Resources and Hydropower Engineering Sciences, Wuhan University, 430072 Wuhan, China
[5]Yellow River Engineering Consulting Co., Ltd. YRCC, 450003 Zhengzhou, China

Received: 3 July 2013 – Accepted: 22 July 2013 – Published: 8 August 2013

Correspondence to: D.-W. Wang (wangdw17@126.com)

Published by Copernicus Publications on behalf of the European Geosciences Union.

Abstract

Floods caused by levee breaching pose disastrous risks to the lower reaches and the flood flow zones of rivers. Thus, a comprehensive assessment of flow and sediment transport during floods must be performed to mitigate flood disasters. Given that the flow state becomes relatively more complex and the range of the submerged area becomes more extensive after a levee breach, this paper established a flow and sediment model by using two-dimensional shallow water equations (SWEs) to explore the break development process and the flow and sediment transport in a curved bed after a levee breach due to overtopping. A three-element weighted essentially non-oscillatory-Roe scheme was adopted for the discretization of SWEs. In addition, a non-equilibrium total-load sediment transport model was established to simulate the scour depth development process of the break. A stable equilibrium of the break was established based on flow shear force and soil shear strength. The lateral widening of the break was simulated by the scouring-collapse lateral widening mode. These simulations, together with the levee breach experiment conducted in the laboratory, demonstrate the validity of the flow and sediment transport process established in this paper. The effects of waterhead in and out of the watercourse, the rate of flow, the levee sediment grading, and other variables during levee breaching were also analyzed. The mathematical model calculation provided a number of physical quantities, such as rate of flow and flow state at the break, that are difficult to measure by using the current laboratory facilities. The results of this research provide fundamental data for developing measures that can reduce casualties and asset loss due to floods caused by levee breaching.

1 Introduction

Floods caused by levee breaching due to overtopping can cause major disasters. Thus, many scholars have indicated the importance of studying this area. To date, a considerable number of fruitful studies have been conducted (Morris, 2009). Risk assessment is

NHESSD

1, 3935–3965, 2013

a crucial premise for the mitigation of flood disasters. However, the flood development process, which is crucial to flood from levee breaching, must first be understood before flood risk assessment can be conducted (Apel et al., 2006). The use of mathematical models to calculate flood from levee breaching is currently a focus of several research (Wu and Wang, 2007, Wu et al., 2012; Yu et al., 2009; Savant et al., 2010; Liu and Wu, 2011; Chen, 2013). After a levee breach, the sudden burst of the watercourse flow leads to an increase in the downstream water level, consequently forming a discontinuity wave. Certain physical parameters of the flow generate gaps on the discontinuity surface. The commonly used numerical method of solving shallow water equations (SWEs) often fails or loses stability in calculating the water flow rate in a levee breach or presents non-physical oscillation issues because of the characteristics of the discontinuity wave. Smoothing the discontinuity results in a low resolution ratio (Toro, 2001). A weighted essentially non-oscillatory (WENO) scheme was integrated with the Roe scheme to overcome the limitations of conventional calculation patterns. Several numerical experiments have verified the capability of the WENO–Roe scheme to differentiate and capture shock waves accurately (Shu, 2003). This method has also been employed in a study on improving the calculation accuracy of a shallow water model.

In levee breach calculations, changes in details, such as local flow of break mouth, topographical changes, and mouth lateral widening velocity, should be accurately recorded. Thus, the mathematical model of a levee breach requires an accurate flow calculation and a precise simulation of break development. Most existing studies consider dikes or levees as homogeneous materials. The development of break can generally occur in two ways: instant collapse and progressive collapse. For an instant collapse, the break is assumed to have formed instantly, and the form of break is difficult to change. The numerical simulation of concrete levees or stonemason levees can only handle simpler situations. However, in reality, a progressive collapse is the more frequent cause of levee breaching. Thus, if the lateral widening of the break is ignored, and the instant collapse of the earth dike is assumed, then more significant errors will be generated. However, given the complexity of the problem, researchers generally

NHESSD
1, 3935–3965, 2013

provide assumptions for the break position and shape when developing simulations. If the initial shape of the break is more regular and the section in its development process is uniformly eroded, then the initial shape is maintained. For example, if the initial break is triangular, rectangular, trapezoidal, or parabolic, the shape is maintained, and only the enhanced breaking or depth is shown. In 1965, Cristofano (1973) established the first numerical simulation of progressive erosion and earth-rockfill levee breaching. The width of the break with trapezoidal shape remained unchanged in the model. In addition, only the vertical erosion and scouring were considered, and the maximal scouring reached only the bedrock. The scouring of the side slope was not considered. The lateral widening of the levee started from the vertical erosion and scouring to the side slope collapse. In contrast to the sediment amount in the flow, the sediment amount from the side slope collapse can be neglected. The fluted bed slope was equal to the internal friction angle of earth fills. Harris and Wagner (1967) executed the following modifications on the model developed by Cristofano: the top width was 3.75 times the length of the depth, the side slope had a parabolic form of approximately 45°, and the erosion of the break was assumed to develop at the bottom of the dam. During the 1980s, Lou (1981) proposed a mathematical model of a progressive collapse of an earth-rock dam caused by overtopping. The most distinctive feature of this model was that the break form was not assumed without previous notice, and the analytical solution of the break form was deducted from the shear stress and the erosion mechanism. Nogueira (1984) also presented a model similar to Lou's. The most significant difference between the two models was the means of identifying the break shape. In the model by Nogueira, the shape of the transverse section of the fluted break was identified by the effective shear stress, that is, the difference between the total shear stress at a point and the critical shear stress. In 1984, Fread (1988) successfully developed the DAMBRK model, which required fewer parameters to identify the break shape. In this model, the initial break shape can be identified with a single parameter. The break shape, including the rectangular, triangular, and trapezoidal shapes, can be identified by adjusting this single parameter. The ultimate break size was determined

NHESSD
1, 3935–3965, 2013

by the final bottom width of the break. However, the specific calculation of sediment transportation was not included in this model. The break development process was assumed to evolve with linear velocity over time. In the subsequent BREACH model developed by Fread (1988), the identification method of the break shape and the break development process were improved. Fread provided two methods for further application. The first method assumed the initial break shape as a rectangle, whereas the other method involved the deduction of the break width on the basis of slope stability. A collapse happens when the undercut depth of the break reaches the critical depth. The critical depth depends on the internal friction angle, the cohesive force, the angle formed by the lateral and horizontal directions of the break, and the density of the levee materials. Faeh (2007) adopted the 2-D flow and sediment model to simulate the flow rate of the break in levee breaching due to overtopping and assessed the effect of each parameter on the flow rate of the break. Wu et al. (2012) applied the Harten, Lax and van Leer (HLL) Riemann Solver with second-order accuracy to simulate the levee breaching process of a non-cohesive soil embankment.

These various levee breach models primarily propose three assumptions: (1) the break shape remains unchanged; (2) the break section in the break development was scoured homogeneously; (3) the materials of the levee were homogeneous. These assumptions have slight inconsistencies with reality, which reduces the reliability of the calculation results. A non-equilibrium total-load sediment transport model and the scouring-collapse mode of break lateral widening were established based on the high-precision numerical format in calculating the flow from levee breaching to simulate the scour depth and lateral widening of break development. In addition, levee breaching experiments were conducted, and the results verified the capability of this method to calculate the flow and sediment transport of the levee breach. The effects of parameters, including water-head in and out of the course, rate of flow, and levee sediment grading, during levee breaching were analyzed. A number of physical quantities that are difficult to measure using the existing experimental methods, such as the rate of flow at the break and the flow regime, were supplemented.

NHESSD
1, 3935–3965, 2013

2 Methods

2.1 WENO–Roe method for shallow water equation

The diffusion term can be ignored in the WENO–Roe method because of the specific characteristics of levee breach flow and the dominant role of the convection. Thus, to consider the drastically topographic changes in the levee breaching process and the enormous sediment concentration in the flow, the fundamental equation adopted the conservation form (Wu et al., 2012)

$$\frac{\partial \boldsymbol{U}}{\partial t} + \frac{\partial \boldsymbol{F}}{\partial x} + \frac{\partial \boldsymbol{G}}{\partial y} = \boldsymbol{S}(\boldsymbol{U}), \tag{1}$$

where $\boldsymbol{U} = \begin{bmatrix} \rho h \\ \rho hu \\ \rho hv \end{bmatrix}$; $\boldsymbol{F} = \begin{bmatrix} \rho hu \\ \rho hu^2 + \frac{1}{2}\rho g h^2 \\ \rho huv \end{bmatrix}$; $\boldsymbol{G} = \begin{bmatrix} \rho hv \\ \rho huv \\ \rho hv^2 + \frac{1}{2}\rho g h^2 \end{bmatrix}$;

$$\boldsymbol{S} = -\begin{bmatrix} \rho_b \frac{\partial z_b}{\partial t} \\ gh\left(s_x - f_x - \frac{1}{2}h\frac{\partial \rho}{\partial x}\right) \\ gh\left(s_y - f_y - \frac{1}{2}h\frac{\partial \rho}{\partial y}\right) \end{bmatrix};$$

t represents time; x and y represent the longitudinal and the lateral coordinates, respectively; h represents the flow depth; u and v represent the flow velocities along the x and y directions, respectively; $\partial z_b/\partial t$ represents the rate of change in bed surface elevation; z_b represents the bed surface elevation above the reference datum; g represents the gravitational acceleration; ρ represents the density of the water and sediment mixture in the water column determined by $\rho = \rho_w(1 - S_t) + \rho_s S_t$. Here, S_t represents the volumetric concentration of the total-load sediment; ρ_w and ρ_s represent the water and the sediment densities, respectively. ρ_b represents the density of the water and the sediment mixture on the bed surface-layer determined by $\rho_b = \rho_w p_m + \rho_s(1 - p_m)$,

NHESSD
1, 3935–3965, 2013

in which p_m represents the porosity of the surface-layer bed material. s_x and s_y represent the bed slopes along the x and y directions, respectively, which are determined by $s_x = -\frac{\partial z_b}{\partial x}$, $s_y = -\frac{\partial z_b}{\partial y}$. f_x and f_y represent the bed friction due to bed roughness along the x- and y-directions, respectively, which can be estimated by empirical formulation as $f_x = \frac{n^2 u\sqrt{u^2+v^2}}{h^{4/3}}$ and $f_y = \frac{n^2 v\sqrt{u^2+v^2}}{h^{4/3}}$. n represents the Manning roughness coefficient; $m_b = \sqrt{1+\left(\frac{\partial z_b}{\partial x}\right)^2+\left(\frac{\partial z_b}{\partial y}\right)^2}$ is considered the curved bed (bank) surface or perimeter.

On the basis of the Godnnov discretization pattern in the conservation equation, the control Eq. (1) can be discretized into

$$\boldsymbol{U}_{i,j}^{n+1} = \boldsymbol{U}_{i,j}^{n} - \frac{\Delta t}{\Delta x}\left(\boldsymbol{F}^*_{i+\frac{1}{2},j} - \boldsymbol{F}^*_{i-\frac{1}{2},j}\right) - \frac{\Delta t}{\Delta x}\left(\boldsymbol{G}^*_{i,j+\frac{1}{2}} - \boldsymbol{G}^*_{i,j-\frac{1}{2}}\right) - \Delta t\boldsymbol{S}, \tag{2}$$

where $\boldsymbol{F}^*_{i\pm\frac{1}{2},j}$ and $\boldsymbol{G}^*_{i,j\pm\frac{1}{2}}$ represent the flux value at the interface formed by the x and y directions, respectively; Δt is the time step; Δx and Δy represent the spatial step along the x and y directions, respectively. The grid is shown in Fig. 1.

Equation (2) can be solved by accurately building the numerical flux of the interface as $\boldsymbol{F}^*_{i\pm\frac{1}{2},j}$, $\boldsymbol{G}^*_{i,j\pm\frac{1}{2}}$, from which high-precision conserved variables can be established. The goal of the WENO scheme is to solve for the values of the conservation variables at both sides of the unit interface to obtain the numerical flux at the interface. First, the unit number contained by the template must be identified because high resolution and high precision can be achieved by increasing the unit number in the template. Given the complexity of the computation, a three-unit template, which can reach the fifth order, was used. Thus, the weight coefficient w_r can be expressed as

$$w_r = \frac{\alpha_r}{\sum_{s=0}^{k-1}\alpha_s}, \quad r = 0,\cdots,k-1, \alpha_r = \frac{d_r}{(\varepsilon+\beta_r)^2}, \tag{3}$$

NHESSD
1, 3935–3965, 2013

where β_r is the smooth factor; $\varepsilon > 0$ and a minimal value is generally obtained to prevent the denominator from becoming zero. In this paper, the value of ε was 10^{-6}.

The difficulty in numerically solving the Riemann discontinuous decomposition is caused by the complexity of the discontinuous decomposition generated by nonlinearity. The Roe method was used to apply the conservation variable of the adjacent constant states to derive a rational linear matrix that can replace the complex nonlinear matrix. In this way, the complex nonlinear issue was transformed into a linear issue. After linearization, the characteristics of the numerical flux can be presented as

$$\boldsymbol{F}^*_{i+\frac{1}{2},j} = \frac{1}{2}\left(\boldsymbol{F}_{i+\frac{1}{2},j}(\boldsymbol{U}_l) + \boldsymbol{F}_{i+\frac{1}{2},j}(\boldsymbol{U}_r) - \sum_{k=1}^{3}\widetilde{\alpha}_k|\lambda_k|\widetilde{\boldsymbol{e}}_k\right). \quad (4)$$

On the basis of the principles mentioned above, each feature quantity can be obtained from Eq. (4) as follows:

$$\alpha_1 = \frac{1}{2c}\left[\Delta(hu) - (\widetilde{u}-c)\Delta h\right], \alpha_2 = \frac{1}{c}\left[\Delta(hv) - \widetilde{v}\Delta h\right], \alpha_3 = \frac{1}{2c}\left[(\widetilde{u}+c)\Delta h - \Delta(hu)\right];$$

$$\lambda_1 = \widetilde{u}+c, \lambda_2 = \widetilde{u}, \lambda_3 = \widetilde{u}-c;\ \boldsymbol{e}_1 = \begin{bmatrix}1\\ \widetilde{u}+c\\ v\end{bmatrix}, \boldsymbol{e}_2 = \begin{bmatrix}0\\ 0\\ c\end{bmatrix}, \boldsymbol{e}_3 = \begin{bmatrix}1\\ \widetilde{u}-c\\ v\end{bmatrix},$$

where $\widetilde{u} = \frac{\sqrt{h_r}u_r + \sqrt{h_l}u_l}{\sqrt{h_l}+\sqrt{h_r}}$, $\widetilde{v} = \frac{\sqrt{h_r}v_r + \sqrt{h_l}v_l}{\sqrt{h_l}+\sqrt{h_r}}$, $c = \frac{\sqrt{gh_r}+\sqrt{gh_l}}{2}$ are Roe's average, and $\boldsymbol{\Delta U} = \boldsymbol{U}_r - \boldsymbol{U}_l$ represents the increase in values of the conservation variables at both sides of the interface. Similarly, the Roe reference vectors along the y direction can be obtained to form $\boldsymbol{G}^*_{i,j+\frac{1}{2}}$.

The third-order Runge–KuttaTVD method and the slop flux method were adopted to process the source term to ensure the accuracy and the stability of the calculation (Wang et al., 2012).

NHESSD
1, 3935–3965, 2013

2.2 Bed scouring and lateral widening of the break

2.2.1 Bottom scouring simulation

For the bed scouring of the break, the inhomogeneous and imbalanced sediment transfer mode was used in the calculation, and the basic equations are presented as follows:

Continuity equation of the sediment:

$$\frac{\partial(hS_k)}{\partial t}+\frac{\partial(huS_k)}{\partial x}+\frac{\partial(hvS_k)}{\partial x}+\rho'\frac{\partial z_{bsk}}{\partial t}=\frac{\partial}{\partial x}\left(D_s\frac{\partial(hS_k)}{\partial x}\right)+\frac{\partial}{\partial y}\left(D_s\frac{\partial(hS_k)}{\partial y}\right) \quad (5)$$

Suspended sediment deformation equation:

$$\rho_b\frac{\partial z_{bsk}}{\partial t}=\alpha\omega_k(S_k-S_{*k}) \quad (6)$$

Bed-load deformation equation:

$$\rho_b\frac{\partial z_{bgk}}{\partial t}+\frac{\partial g_{bxk}}{\partial x}+\frac{\partial g_{byk}}{\partial y}=0 \quad (7)$$

where ρ_b represents the dry density of the riverbed sludge; D_s represents the sediment diffusion coefficient; S_k represents the sediment content in the k-th group; S_{*k} represents the flow sediment-carrying capacity in the k-th group; z_{bsk} and z_{bgk} represent the river bed elevation change caused by the movement of the suspended load and the bed load in the k-th group, respectively; g_{bxk} and g_{byk} represent the transport rate per unit of the bed load along the x and y directions in the k-th group, respectively; α represents the saturation recovery coefficient. The discretization of the equation adopted the semi-implicit upwind scheme of discretization (Wang et al., 2007).

2.2.2 Lateral widening mode of the break

The collapse-lateral widening mode was adopted to simulate the lateral widening of the break. Instead of needing the differentiated interface between cohesive soil and

NHESSD
1, 3935–3965, 2013

non-cohesive soil, the part of the levee under the water was subjected to lateral scouring, whereas the part above the water was subjected to the lateral widening from the suspending collapse. Based on the experiment, a part of the sediments produced from the collapse were removed by the flow. The rest were piled on the bed according to the underwater slope of repose α of flowing water.

Figure 2 shows the generalized lateral mode based on existing research results and experimental observations.

In Δt, the recession distance of the cohesive soil bank caused by the lateral scouring from the flow was

$$\Delta B = \frac{C_l \cdot \Delta t \cdot (\tau - \tau_c) e^{-1.3\tau_c}}{\gamma_{bk}}, \quad (8)$$

where γ_{bk} is the unit weight of riverbank soils (kN m^{-3}); ΔB is the distance of the bank recession from the lateral widening of the flow lateral scouring in Δt (m); τ is the flow shear stress on the bank (N m^{-2}); τ_c is the start-up shear stress of riverbank soils (N m^{-2}); C_l is the coefficient of lateral scouring, which is related to the physical and chemical properties of riverbank soils. According to the test results, $C_l = 3.6 \times 10^{-4}$, which was basically the same as the results proposed by Osman and Thorne (1988).

$$\tau = \gamma \frac{U^2}{C^2}$$

Here, the resultant velocity is $U = \sqrt{u^2 + v^2}$; γ is the bulk density of the water; C is the Chezy coefficient, which can be obtained by the Manning formula.

For τ_c, the critical drag force equation of the Shields coarse sediment was

$$\tau_c = k(\gamma_s - \gamma)d,$$

where k is the coefficient ranging from 0.04 to 0.06, γ_s is sediment bulk density, and d is the sediment particle size.

NHESSD
1, 3935–3965, 2013

Given that the lower embankment recessed because of flow scouring, the upper part was suspended (see Fig. 2b). When the stress on the upper part of the fracture interface reached the strength of extension, the applied moment produced by the suspended deadweight W created a balance with the stretching resistance produced by the fracture surface to derive the mechanical equilibrium equation. Thus, the equation of the critical overhang length of the river bank can be expressed as follows:

$$L_c = \left(T_0 \cdot H/3\gamma_2\right)^{1/2}, \quad (9)$$

where H, B, γ_2, and T_0 represent the height, the width, the density, and the strength of extension of the soils, respectively.

When $L < L_c$, the cohesive soil layer of the upper part of the riverbank stayed stable and did not collapse. The flow can keep a non-cohesive soil layer.

When $L = L_c$, the cohesive soil layer of the upper part of the riverbank reaches a critical extension value, and a collapse is about to occur.

When $L > L_c$, the cohesive soil layer of the upper part of the riverbank might have collapsed. The critical state of collapsing can be achieved by adjusting the time step.

2.2.3 Introduction of flume experiments

The experiment was conducted in a glass flume of a 180° curved bed (bank). The flume was 1.2 m wide, the bed slope was 1 %, and the radius of the inner curve was 1.8 m. As shown in Fig. 3, a 20 cm wide rectangle break was created at the 4# section (4# section as axis), the elevation of which is lower than the elevation of both sides of the riverbank by 1.5 cm. In the experiment, this rectangle break was used as the break of the levee breach. When the water level was raised to a certain height, the flow was effused from the induced break, and the levee started to outburst.

A water level meter was set up at each section from the upstream to the downstream of the flume to observe the variation in the water level in and out of the riverbank after the levee breach. A total of nine sets were deployed. Each water level meter was

NHESSD
1, 3935–3965, 2013

set to record the local water level every 2 s. The sections of the flume were set as follows: 1# at the upstream straight section, 2# at the curve top, 3# at the upstream of the induced break of the outer river, 4# at the induced break of the outer river, 5# at the end of the curve section of the outer river, 6# and 9# at the downstream straight section of the inner river, 7# around the stern door of the outer river, and 8# near the stern door of the inner river to deduct the rate of flow in the levee breach. In addition, a graphometer, which can measure the real-time elevation changes in the break, was set in the downstream area of the 4# section of the levee to observe the vertical development process of the break after levee breaching. The layout chart of the experiment is depicted in Fig. 3.

Inhomogeneous sediments comprising two grading levels were used as levee materials to determine the effect of the levee material on the levee breaching process. The grading curves of the sediments are shown in Figs. 4 and 5. The medium-sized particle among the relatively coarse sediments was approximately 0.6 mm (Fig. 4), whereas that of the refined group was approximately 0.4 mm (Fig. 5).

3 Results

3.1 Changing process of water level

Figure 6 shows that the water level meters at the 4# and 6# sections were set on both sides near the break. These water level meters recorded the variation in water level during the levee breaching process. The instant levee water-head at the breach of the inner and the outer river (4# and 6#) reached a maximal value. The flow of the outer river was rapidly elevated in the inner river, which flowed down from the break. The water-head in and out of the river gradually decreased as the break width gradually expanded. In the levee breach, the water level of the outer river declined steadily, whereas that of the inner river changed drastically, from initially reaching the maximal level to gradually declining to a stable level. The flow state of the breach was

NHESSD
1, 3935–3965, 2013

complex. Experiments reveal that the turbulent fluctuation of the flows in the break area became intense. Figure 6 also shows that the water level fluctuation at 6# was intense. The calculation results were generally consistent with the overall experimental results, verifying the feasibility of this numerical simulation.

3.2 Flow structure and quantity of break

The classic flow field near the break is presented in Fig. 7. Figure 7a shows that at 10 s after the levee breach and overtopping, the flow of the outer river was imported into the inner river at the break from the outer river. The flow direction was vertical to the break and was split into two when the flow crushed on the wall of the curved bed (bank). Most of the flows went into the downstream along the curved bed (bank). The bending direction of a few flows was blocked by the wall, forming vortexes. Figure 7b shows that at 50 s, the break flow direction turned to the downstream of the inner river, forming an intersection angle with the break. As the break continued to expand, the flow velocity at the right side of the break of the outer river became smaller than that at the left side, whereas the flow velocity at the right side of the break of the inner river became smaller than that at the left side. The break flow scoured the break and removed the bed sediments. On both sides of the break wall, the instability and the collapse of the soils resulted in the continuing lateral widening of the break. The inner river had dry wash at the initial moment. The break flow then poured from the break into the inner river. Potential energy was rapidly transformed into kinetic energy. The greater the break flow velocity was, the faster the break expanded because of the strong scouring effects. As the water-head in and out of the river and the break lateral widening shrank, the break flow velocity was gradually reduced. As shown in Fig. 7c and d, the velocity of break lateral widening was slowed down progressively.

Torrents of water flow were formed during the levee breaching process. Measuring the rate of flow near the break is difficult. Thus, a mathematical model was used to calculate the rate of flow near the break. As the break expanded after flow overtopping, the rate of flow through the break increased, gradually reaching a peak value.

NHESSD
1, 3935–3965, 2013

The oscillation was reduced, and the rate of flow finally stabilized. Owing to the straight flow and the one-sided break on the watercourse in this experiment, the rate of flow was mostly stabilized and over half of the total rate of flow passed in the watercourse. Figure 8 shows that the water-head in and out of the levee was 18 cm and 15 cm, respectively, when the rate of inflow was 11.57 $L s^{-1}$. The rate of flow of the break is also shown in the figure. As shown in the figure, the break rate of flow sharply increased after the levee breach. At about t = 60 s, the rate of flow into the floodway district reached the peak value. When the water-head in and out of the course was h = 18 cm, the peak rate of the flow through the break was 6.97 $L s^{-1}$, accounting for 60.2 % of the total rate of flow of the watercourse. When h = 15 cm, the peak rate of flow of the break was reduced to 6.01 $L s^{-1}$, accounting for 51.9 % of the total rate of flow of the watercourse. After reaching the peak rate of flow, the water-head at both sides were gradually reduced, consequently reducing the rate of flow through the break. The rate of flow was finally stabilized to 4.04 and 3.83 $L s^{-1}$. Most of the flows flowed downstream through the original watercourse.

3.3 Changing process of the break

After flow overtopping, the levee top was quickly weakened by the effects of the flows, which initially formed rills. Soils at both sides gradually collapsed because of the lateral widening. The mouth development process in the burst is shown in Fig. 9.

Figure 10 shows the undercutting process through break simulation. As shown in the figure, at about 20 s at the beginning of the levee breach, the elevation of the levee top dropped drastically from 15 cm to approximately 8 cm. The decreasing velocity of the elevation of the levee top was significantly slowed down and stabilized at 4 cm. At the end of the experiment, the maximal height of the measured elevation was approximately 3.8 cm, which is generally consistent with the simulation results.

On the basis of the plane modality, the break width on one side of the watercourse in the floodway district was wider than that on the other side. The top width of the break on one side was larger than the bottom width, which can be attributed to the

NHESSD
1, 3935–3965, 2013

soil accumulation on the bottom of the break after the suspension and collapse, consequently shrinking of the bottom width of the break. As the water level and the flow velocity stabilized, the break width gradually stabilized. Erosion and deposition of sediments eventually reached a balance. Comparison between the actual stabilized break width and the calculated stabilized break width revealed that the maximal relative error between the two did not exceed 5 %, indicating the validity of the model adopted in this study.

Figures 11–13 show the break width changing process in the watercourse simulated in different conditions. As shown in the figures, the lateral widening did not start during the flow overtopping, but occurred after a period of time. The break expansion velocity and the stabilized width were positively correlated with the rate of flow Q in the watercourse. The levee body piled by coarse sediment particles was scoured by the flow and had smaller lateral widening velocity. Finally, no significant difference was observed between the stable break width and the break width of the levee piled by refined sediments. During the levee breach, the water-head h at both sides of the watercourse determined the widening rate. The greater the h was, the greater was the velocity of lateral widening of the break. Thus, a larger stable break width can be finally formed.

4 Conclusions

In the paper, a mathematical model that can calculate the flow and sediment transport in levee breach was established. This model can accurately reflect the water level changing process on both sides of the watercourse after levee breaching by analyzing the flow velocity distribution, the scouring, and the widening of the break and discharge. Experimental data on levee breaching proved the effectiveness of the algorithms used in the model and the processing patterns, indicating that the calculation mode adopted in this research can simulate the flow and sediment transport. In addition, the effects of the rate of flow of the watercourse, the water-head in and out of the watercourse, and the material composition of break on the flow and sediment transport were analyzed.

NHESSD
1, 3935–3965, 2013

The water level on one side of the watercourse dropped after the levee breach. The outer water level of the break increased because the outer water was constrained by the walls of the flume. The two water levels gradually grew closer and eventually reached a steady state. However, the water flow process caused by levee breaching in the floodway district was not constrained by walls.

In the sandy soil levee breaching, an etched groove was formed on the top of the levee after flow overtopping. The part of the levee under water was drastically scoured by the flow, resulting in the vertical undercutting and lateral widening. Consequently, that part of the levee was fractured because of the suspension of the levee above the water level, resulting in lateral widening. The lateral widening of the levee was attributed to these two modes. The break lateral widening of the soil levee was accurately simulated in the scouring-collapse lateral widening mode on the basis of the mechanic concepts such as flow sheer force and the shear strength of the soil body.

The rate of flow through the break was closely related to the water-head on both sides of the river and to the break area. Considering the other conditions the same, the final peak rate of flow of the break was positively correlated with the water-head in and out of the watercourse at the beginning of the levee breach. At the beginning of the levee breach, the water-head in and out of the watercourse was relatively large, and the break rapidly expanded. The break rate of flow sharply increased. As the water-head on both sides gradually decreased, the break expansion stabilized. The rate of flow reached a peak value and then reduced gradually until no change in the water level on both sides of the watercourse and the break area was observed. The rate of flow through the break reached a stable value as well.

A model for studying sandy soil levee was established in this paper. The proposed calculation mode of break scour depth and lateral widening can effectively simulate the levee breach of sandy soil levee. The effectiveness of this model in practical levee breach calculation needs further verifications by using field data.

NHESSD
1, 3935–3965, 2013

Acknowledgements. This study is supported by the National Basic Research Program of China (973 Program) and the National Natural Science Foundation of China (NSFC) under grant number of 2011CB403306, 51209221, and 11272240 respectively.

References

Apel, H., Thieken, A. H., Merz, B., and Blöschl, G.: A probabilistic modelling system for assessing flood risks, Nat. Hazards, 38, 79–100, 2006.

Chen, W. B., Liu, W. C., and Wu, C. Y.: Coupling of a one-dimensional river routing model and a three-dimensional ocean model to predict overbank flows in a complex river–ocean system, Appl. Math. Model., 37, 6163–6176, 2013.

Cristofano, E. A.: Method of Computing Erosion Rate for Failure of Earthfill Dams, US Department of the Interior, Bureau of Reclamation, Engineering and Research Center, Washington, DC, 1973.

Faeh, R.: Numerical modeling of breach erosion of river embankments, J. Hydraul. Eng.-ASCE, 133, 1000–1009, 2007.

Fread, D. L.: DAMBRK: the NWS dam-break flood forecasting model, Vol. 4, Hydrologic Research Laboratory, National Weather Service, NOAA, Maryland, 1984.

Fread, D. L.: BREACH, an erosion model for earthen dam failures, Hydrologic Research Laboratory, National Weather Service, NOAA, Maryland, 1988.

Harris, G. W. and Wagner, D. A.: Outflow from Breached Earth Dams, BSc. thesis, University of Utah, Salt Lake City, Utah, 1967.

Liu, W. C. and Wu, C. Y.: Flash flood routing modeling for levee-breaks and overbank flows due to typhoon events in a complicated river system, Nat. Hazards, 58, 1057–1076, 2011.

Lou, W. C.: Mathematical Modelling of Earth Dam Breaches, Colarado State University, Fort Collins, Colorado, USA, 1981.

Morris, M. W., Kortenhaus, A., and Visser, P. J.: Modelling breach initiation and growth, FLOODsite Report T06-08-02, FLOODsite, 2009.

Nogueira, V. A.: Mathematical Model of Progressive Earth Dam Failure, Colarado State University, Fort Collins, Colorado, USA, 1984.

Osman, A. M. and Thorne, C. R.: Riverbank stability analysis I: theory, J. Hydraul. Eng.-ASCE, 114, 134–150, 1988.

NHESSD

1, 3935–3965, 2013

Savant, G., Berger, C., McAlpin, T. O., and Tate, J. N.: Efficient implicit finite-element hydrodynamic model for dam and levee breach, J. Hydraul. Eng.-ASCE, 137, 1005–1018, 2010.

Shu, C. W.: High-order finite difference and finite volume WENO schemes and discontinuous Galerkin methods for CFD, Int. J. Comput. Fluid D., 17, 107–118, 2003.

Toro, E. F.: Shock-Capturing Methods for Free-Surface Shallow Follows, John Wiley, Chichester, New York, 2001.

Wang, D. W., Yang, G. L., Yu, M. H., Wang, M., and Dou, S. T.: A new semi-implicit scheme for two-dimensional convection equation, Engineering Journal of Wuhan University, China, 40, 18–21, 2007.

Wang, D. W., Liu, X. F., Chen, J. G., and Ji, Z. W.: The slop flux method for numerical balance in using Roe's approximate Riemann solver, J. Hydrodyn., 24, 58–64, 2012.

Wu, W. and Wang, S. S. Y.: One-dimensional modeling of dam-break flow over movable beds, J. Hydraul. Eng.-ASCE, 133, 48–58, 2007.

Wu, W., Marsooli, R., and He, Z.: Depth-averaged two-dimensional model of unsteady flow and sediment transport due to noncohesive embankment break/breaching, J. Hydraul. Eng.-ASCE, 138, 503–516, 2012.

Yu, M. H., Deng, Y. L., Qin, L. C., Wang, D. W., and Chen, Y. L.: Numerical simulation of levee breach flows under complex boundary conditions, J. Hydrodyn., 21, 633–639, 2009.

NHESSD

1, 3935–3965, 2013

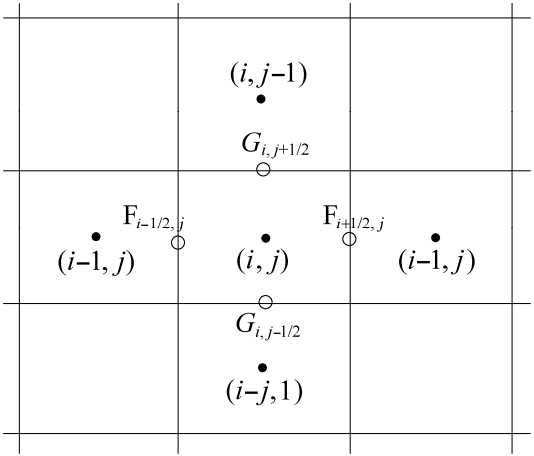

Fig. 1. Solution grid.

NHESSD
1, 3935–3965, 2013

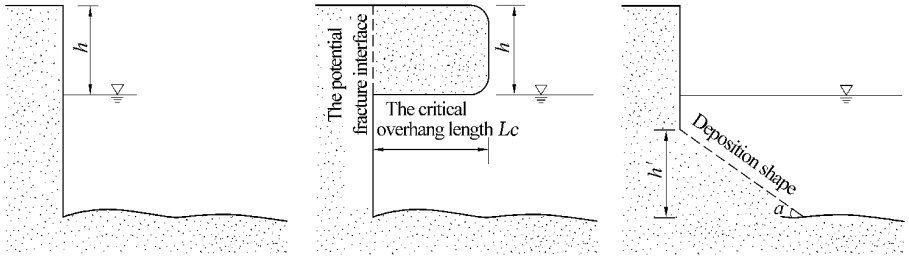

(a) initial (b) lateral scouring (c) bund collapse

Fig. 2. Lateral widening mode of the break.

NHESSD
1, 3935–3965, 2013

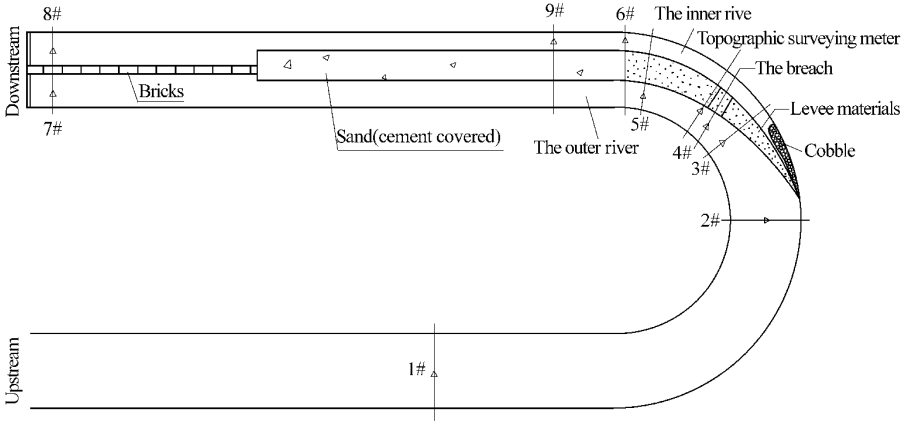

Fig. 3. Sketch of the experiment layout.

NHESSD
1, 3935–3965, 2013

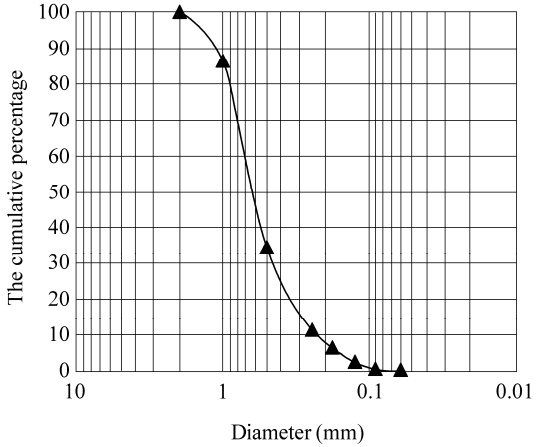

Fig. 4. Coarse sand grading curve.

NHESSD
1, 3935–3965, 2013

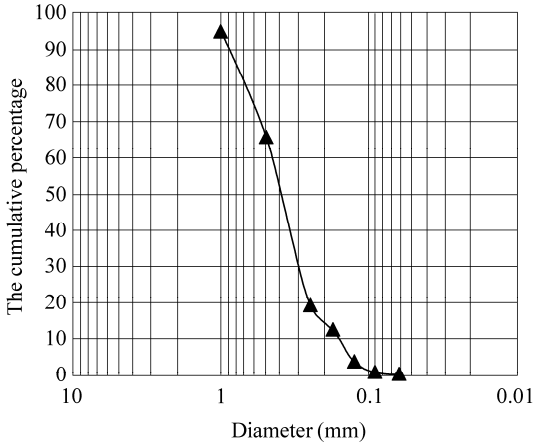

Fig. 5. Fine sand grading curve.

NHESSD
1, 3935–3965, 2013

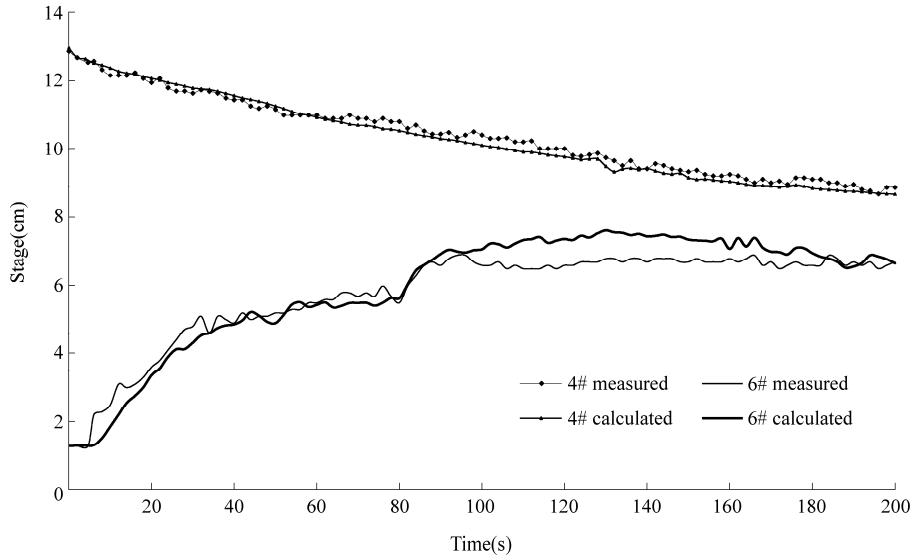

Fig. 6. Comparison between the calculated water level and actual water level.

NHESSD
1, 3935–3965, 2013

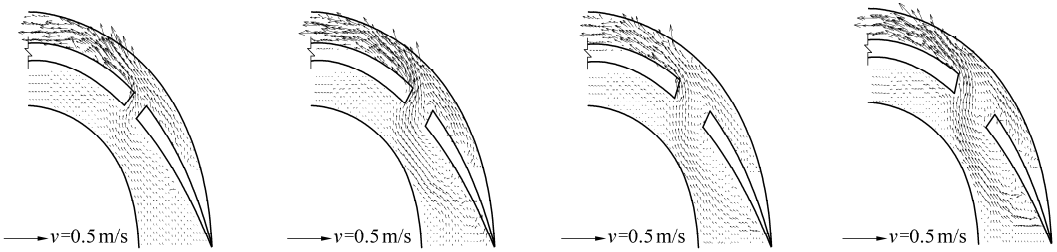

(a) t=10 s (b) t=50 s (c) t=100 s (d) t=100 s

Fig. 7. Typical flow field near the break.

NHESSD
1, 3935–3965, 2013

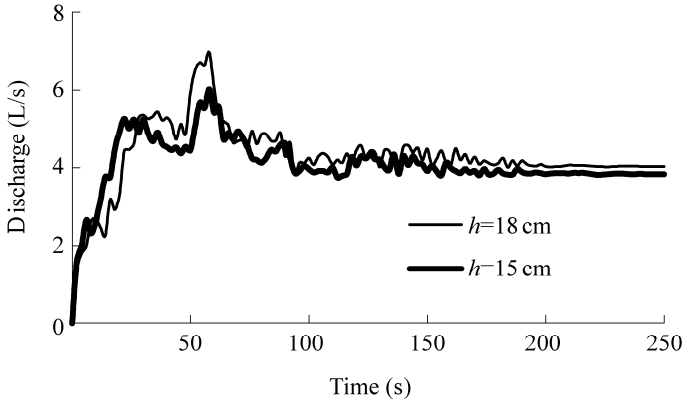

Fig. 8. Calculation of the break rate of flow.

NHESSD
1, 3935–3965, 2013

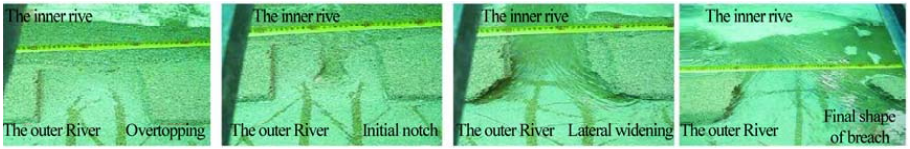

Fig. 9. Mouth development process in the levee breach.

NHESSD
1, 3935–3965, 2013

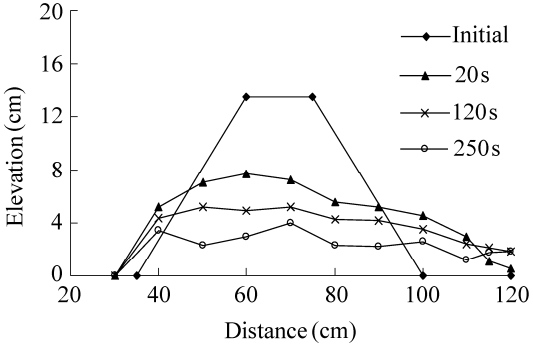

Fig. 10. Changing process of the longitudinal profile of the break.

NHESSD
1, 3935–3965, 2013

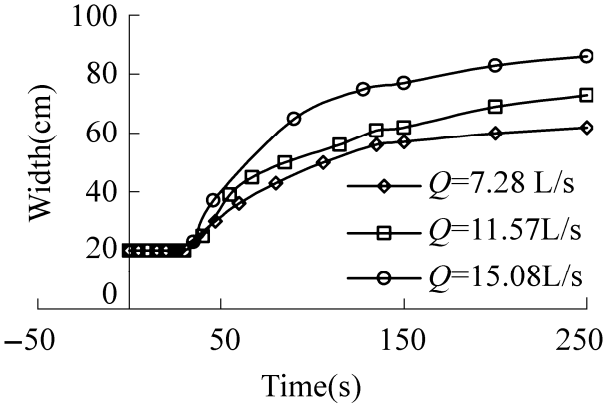

Fig. 11. Relationship between the break width changing process and rates of flow.

NHESSD
1, 3935–3965, 2013

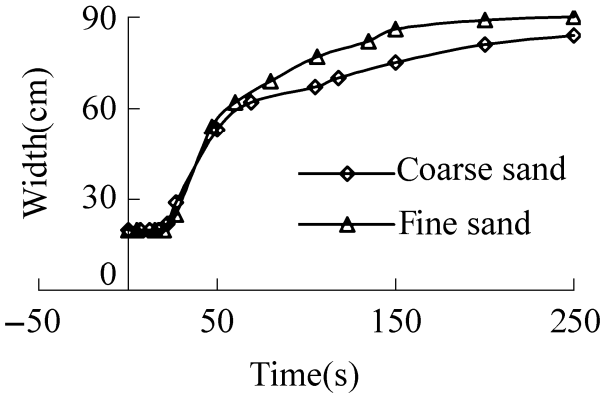

Fig. 12. Relationship between break width and sediment grading.

NHESSD
1, 3935–3965, 2013

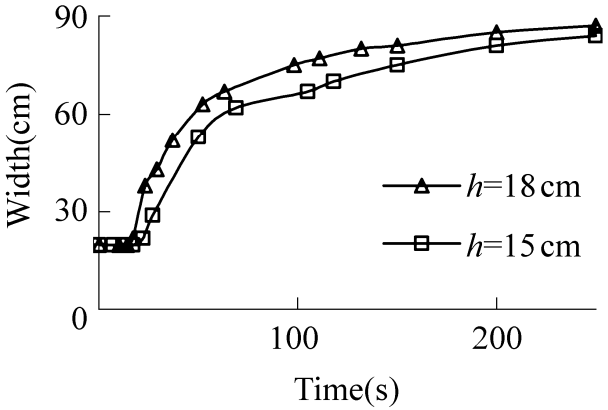

Fig. 13. Relationship between break width and water-head in and out of the course.

NHESSD
1, 3935–3965, 2013